minerals

MDPI

Article

Sulfate Sources Required for Thermochemical Sulfate Reduction in Dolostone Reservoirs in the Upper Permian Changxing Formation, Yuanba Gas Field, Sichuan Basin, China: Insights from the Origin of Celestite

Xinya Yu [1,*], Dancheng Zhu [2], Huayao Zou [2] and Fang Hao [3]

[1] School of Earth Resources, China University of Geosciences, Wuhan 430074, China
[2] College of Geosciences, China University of Petroleum, Beijing 102249, China; foreverimage@126.com (D.Z.); huayaozou@cup.edu.cn (H.Z.)
[3] School of Geosciences, China University of Petroleum, Qingdao 266580, China; haofang@upc.edu.cn
* Correspondence: xinyayu1220@163.com

Abstract: Thermochemical sulfate reduction (TSR) commonly occurred in the dolostone reservoirs of the Upper Permian Changxing Formation (P_3c) in the Yuanba (YB) gas field, Sichuan Basin, yet controversy remains regarding the source of sulfate required for TSR. To trace the source of the sulfate, sulfur and strontium isotopic compositions were measured for three diagenetic celestite ($SrSO_4$) samples found in the P_3c dolostone reservoirs in the YB gas field. In addition, the sulfur isotopic compositions of Carbonate-associated sulfates (CAS) from the P_3c carbonates and spheroidal pyrites in dolomicrites from the P/T boundary (PTB) in the YB gas field were measured for comparative studies. The results show that the sulfur isotopic compositions of celestites are significantly heavier than those of the contemporaneous seawater, and these celestites have strontium isotopic values consistent with those of the host dolostones and contemporaneous seawater. The −33.68‰ fractionation in average $\delta^{34}S$ values between pyrites and celestites indicated that their formation was likely to be related to bacterial sulfate reduction (BSR). During the P/T extinction event that accompanied the end-Permian regression, the reflux of brine directly precipitated ^{34}S-rich celestites in the fractures and vugs of the dolostone reservoirs due to the BSR and the evaporation of seawater. These ^{34}S-rich celesites and associated pore fluids provide a new explanation for the source of sulfate required for the late TSR.

Keywords: sulfate source; celestite; sulfur isotopes; dolomitization; bacterial sulfate reduction; thermochemical sulfate reduction

check for updates

Citation: Yu, X.; Zhu, D.; Zou, H.; Hao, F. Sulfate Sources Required for Thermochemical Sulfate Reduction in Dolostone Reservoirs in the Upper Permian Changxing Formation, Yuanba Gas Field, Sichuan Basin, China: Insights from the Origin of Celestite. *Minerals* **2022**, *12*, 605. https://doi.org/10.3390/min12050605

Academic Editor: Thomas Gentzis

Received: 7 April 2022
Accepted: 9 May 2022
Published: 11 May 2022

Publisher's Note: MDPI stays neutral with regard to jurisdictional claims in published maps and institutional affiliations.

Copyright: © 2022 by the authors. Licensee MDPI, Basel, Switzerland. This article is an open access article distributed under the terms and conditions of the Creative Commons Attribution (CC BY) license (https://creativecommons.org/licenses/by/4.0/).

1. Introduction

Thermochemical sulfate reduction (TSR) by organic–inorganic interactions in carbonate hydrocarbon reservoirs, particularly those associated with dolostone reservoirs, is one of the common diagenetic interactions and is widely studied due to its highly corrosive nature to production equipment, its toxicity to life, its impact on reservoirs, and its indicative significance in hydrocarbon source and evolution studies [1–7]. In most reported TSR geologic cases, liquid hydrocarbons and natural gases are the explicit primary reducing agents, whereas there are different sources of the oxidizer sulfate, with possible sources including sedimentary anhydrites [8,9], anhydrite cements [10], dissolved sulfates [11–13], dolomitizing fluids [14–16], and carbonate-associated sulfates (CAS) [17–19]. During TSR, inorganic sulfur from oxidant sulfate is incorporated into solid bitumen, H_2S, and some metal sulfides (e.g., pyrite), leading to the enrichment of ^{34}S in these sulfur-bearing species and thus approaching the sulfate isotopic composition of sulfate [1,20–22]. Solid bitumen formed by TSR, for example, typically has sulfur isotopic fractionation values in the range of −15‰ to 0‰ with respect to sulfate [21,23,24]. Therefore, the source of the sulfate

required for TSR can be determined from the sulfur isotopic fractionation values between the sulfur-bearing species formed by TSR and the potential sulfates.

Intense TSR has occurred in the dolostone reservoirs in the Lower Triassic Feixianguan Formation (T_1f), Puguang (PG) gas field, northeast Sichuan Basin, with hydrogen sulfide contents ranging from 5.1% to 62.2% (average 18.4%) [4,5], which is proposed to be related to the evaporative depositional environment of the reservoir rocks [13,25]. However, in the absence of evaporite deposition in the Changxing Formation (P_3c) in the YB gas field, significant TSR still occurred in the large-scale dolostone reservoirs, with hydrogen sulfide contents ranging from 1.2% to 25.7% (average 7.0%) [15]. Regarding the source of sulfates required for the TSR in the P_3c in the YB gas field, Li et al. [26] concluded that the sulfates mainly originated from the fourth member of the Feixianguan Formation (T_1f^4) by comparing the sulfur isotopic compositions of the reservoir solid bitumens in the P_3c with those of the anhydrites in the T_1f^4. In contrast, Tian et al. [27] believed that evaporative fluids from the T_1f_4 and the Jialingjiang Formation (T_1j) were not likely to penetrate the thick and tight limestones at the bottom of the T_1f into the P_3c reef and shoal carbonates. Li et al. [16] argued that the seepage reflux of evaporative seawater in the back-reef lagoons formed dolostone reservoirs during the Late Permian in the YB gas field, and the dolomitization process enriched porewater sulfates, which provided a sulfate source for the later TSR. Therefore, the source of sulfates required for the TSR in the P_3c of the YB gas field remains controversial. This article is based on the study of the origin of three celestite ($SrSO_4$) cements found in the P_3c dolostone reservoirs of the YB gas field to elucidate the source of sulfate required for TSR.

2. Geological Setting

Sichuan Basin is a diamond-shaped basin in southwest China (Figure 1A), which was formed on the basement of the Presinian. The formation of the basin mainly went through two stages [28]. Before the early Indosinian movement, Sichuan Basin was mainly dominated by extensional setting and marine carbonate deposition. After the early Indosinian movement, the tectonic setting turned to compression, and the overall uplift of the Sichuan Basin resulted in the development of terrigenous clastic sediments, which were eventually shaped by folding and uplift during the Yanshanian and Himalayan movements [28].

During the Late Permian, the Sichuan Basin was rifted inside the stable platform of the Early Permian under the influence of the Emei taphrogeny [29]. In the northeast of the Sichuan Basin, a NW-SE continental shelf was formed, and an isolated carbonate platform was formed in the east, while a large platform developed in the west, which is in transition with the ancient land in the southwest (Figure 1A). Surrounding the shelf, several large gas fields have been discovered on the platform on both sides, such as the YB and PG gas fields. During the Late Permian and Early Triassic, the Wujiaping (P_3w) and Changxing (P_3c) formations and the Feixianguan (T_1f) and Jialingjiang (T_1j) formations were deposited in the Sichuan Basin from bottom to top, respectively (Figure 1B). The mudstone hydrocarbon source rocks of the P_3w were deposited inside the shelf due to rifting activities during the early phase of the Late Permian. By the end of the Permian, the reef and bioclastic shoal reservoirs of the P_3c were deposited on the platform on both sides of the shelf. The P_3c can be divided into the first (P_3c^1) and second (P_3c^2) members, which form a third-order shallowing-upward sequence. At the end of the Late Permian, the top of the P_3c was short exposed due to the global sea-level fall [30,31]. During the early Early Triassic, the platform margins were dominated by the deposition of the T_1f oolitic shoals. As the depositional environment varied, anhydrites were deposited within the isolated platform on the east side of the shelf, while no anhydrites were deposited on the open platform on the west side of the shelf (Figures 1 and 2). By the end of the deposition of the T_1f, the entire northeast Sichuan Basin was in a restricted evaporative depositional environment due to further sea-level fall, where several layers of thin anhydrites were deposited. The T_1f can be divided into four members from bottom through top: the first (T_1f^1), second (T_1f^2), third, (T_1f^3) and fourth (T_1f^4) members, of which the T_1f^1 and T_1f^2

and T_1f^3 and T_1f^4 form a third-order shallowing-upward sequence, respectively. By the late phase of the Early Triassic, more restricted evaporative environments were widely developed, resulting in the deposition of the T_1j thick evaporates. The T_1j can be divided into five members, and evaporates are mainly developed in the second to fifth members ($T_1j^{2–5}$).

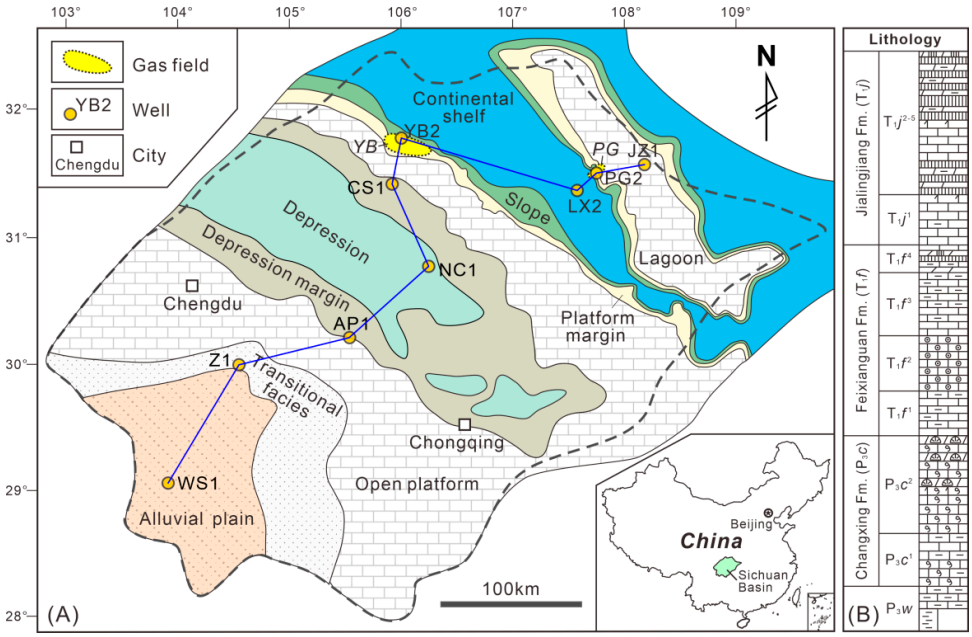

Figure 1. (**A**) Location map showing the Yuanba (YB) gas filed in the Sichuan Basin and sedimentary facies during the deposition of the P_3c (Modified from Du et al. [32]). PG, Puguang gas field. (**B**) Generalized stratigraphy of the Upper Permian and Lower Triassic in the northeast Sichuan Basin. The lithology legends are shown in Figure 2. Fm., Formation.

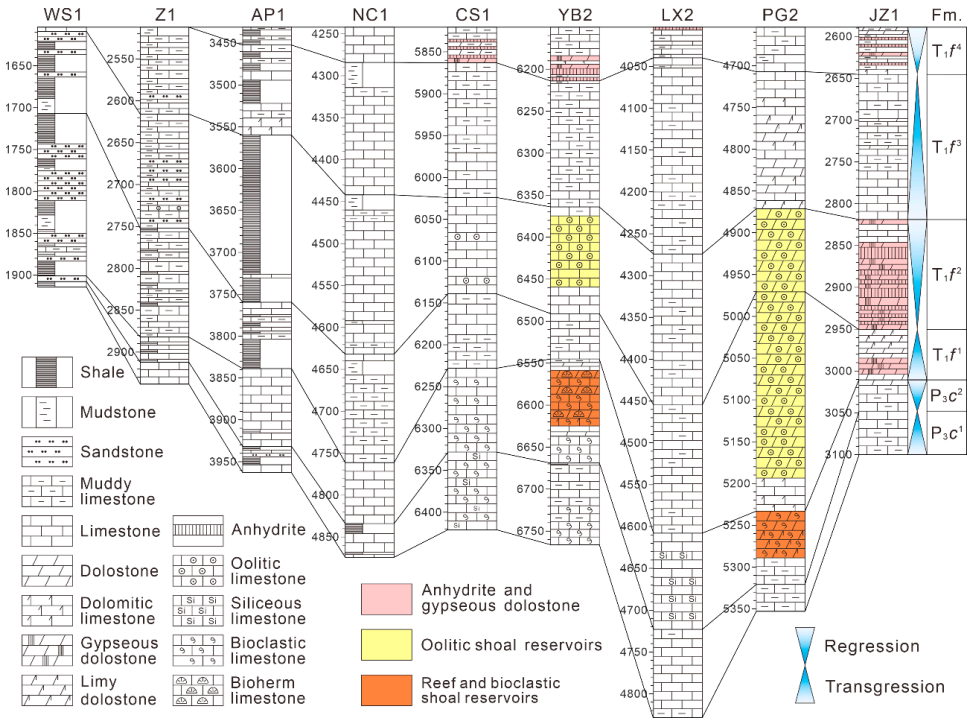

Figure 2. Lithologic variations in the P_3c and T_1f in the Sichuan Basin from southwest to northeast. The well locations are shown in Figure 1A.

The YB gas field, discovered in 2007, is located in the northeast Sichuan Basin in a gentle tectonic zone with weak deformation and a lack of faults [33,34]. The main gas-producing reservoirs are the reef and bioclastic shoal dolostone reservoirs of the P_3c, which commonly contain hydrogen sulfide and sulfur-bearing bitumen [26]. Gases from P_3c in the YB gas field have been proven to be mainly derived from sapropel source rocks of the P_3w [35,36]. Based on reconstructions of burial and thermal histories, the P_3c and T_1f in the northeast Sichuan Basin experienced a maximum burial depth of more than 6000 m and a maximum temperature of more than 180 °C before being uplifted to present-day depths [4,36,37].

3. Materials and Methods

After detailed core observation of the P_3c in the YB gas field, only three celestite samples were obtained from a few wells. To study the origin of these celestites and their petroleum geological significance, several matrix carbonate samples near these celestites from the P_3c as well as pyrite-bearing carbonates at the top of the P_3c were also collected. Petrological and isotopic geochemical analyses were conducted for these samples.

Ten thin sections were prepared for detailed observation on a Nikon Eclipse E600 petrographic microscope. Three polished, platinum-coated thin sections were examined by FEI Quanta 200F scanning electron microscopy (SEM) operating at 10 Kev and 20 nA. The Raman analysis of the fluid inclusions in celestite minerals was conducted on the inVia Reflex micro-Raman instrument developed by Renishaw in the United Kingdom. The solid laser with a laser wavelength of 532 nm and a power of 50 mW was selected.

The sulfur isotopic compositions of three celestite samples, eight extracted carbonate-associated sulfate (CAS) samples, and six extracted pyrite sulfurs from P_3c carbonate rocks were determined. The methods for CAS and pyrite extraction from carbonate rocks are referred to in Li et al. [38] and Jin et al. [39], respectively. The element analyzer (EA, Flash 2000, Thermo Fisher Scientific, Waltham, MA, USA) and isotope mass spectrometer (IRMS, Delta VPlus, Thermo Finnigan LLC, San Jose, CA, USA) were used to determine the sulfur isotopic compositions. Sulfur isotopic compositions are expressed in standard δ-notation as permil (‰) deviation from the V-CDT international standard. The mean standard deviation of the three international standard substances was 0.14‰. The strontium isotopic compositions of three celestite samples, one strontianite sample, and three host dolostone samples were determined on a Triton Ti mass spectrometer (Thermo Finnigan LLC, San Jose, CA, USA) in static mode. Full details of the treatment are referred to in Gao et al. [40] and Xu et al. [41]. The measurements of standard NBS-987 gave $^{87}Sr/^{86}Sr = 0.710228 \pm 0.000007$ (2σ).

4. Results

4.1. Petrography

Core observations reveal that the celestites are fully filling the dissolution fractures and vugs of the dolostones as cements (Figure 3), with the rims replaced by strontianites (Figure 3A,B). Microscopic and SEM observations also show the replacement of celestites by strontianites (Figures 4A–E and 5). A paragenesis of celestites, strontianites, bitumens, and pyrite was found in the P_3c in the YB gas field. It appears that the presence of bitumens led to the alteration of celestites to strontianites, while the pyrites were precipitated in the nearby area (Figure 4E,F). Secondary inclusions distributed along fractures and joints are widely developed in the celestite minerals (Figure 6A), some of which were detected by laser Raman analysis as solid monatomic sulfur and gaseous H_2S (Figure 6B–D), indicating that these celestite minerals have been subjected to TSR alteration. Microscopic and SEM observations showed that spherical pyrites were common in the dolomicrites (about 3 m thick) at the top of the P_3c in the well YB2 from the YB gas field (Figure 7A–F). In addition, terrigenous clay minerals and rounded quartz grains were observed in the microprores of the dolomicrites (Figure 7G).

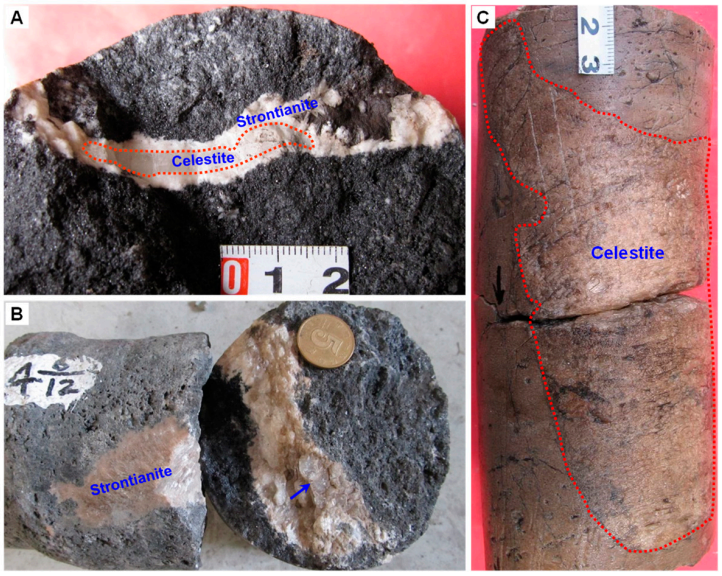

Figure 3. Photographs of drilling cores showing the occurrence of celestites and strontianites in the YB gas field. (**A**) Celestite and strontianite minerals in the fracture of dolostone, 6640.15 m, P_3c, YB29. (**B**) Celestite particles (blue arrow) and strontianite in the dissolution fracture of dolostone, 6461.73 m, P_3c, YB205. (**C**) Celestite mineral completely filled in the dissolution vugs of dolostone, 6583.10 m, P_3c, YB2.

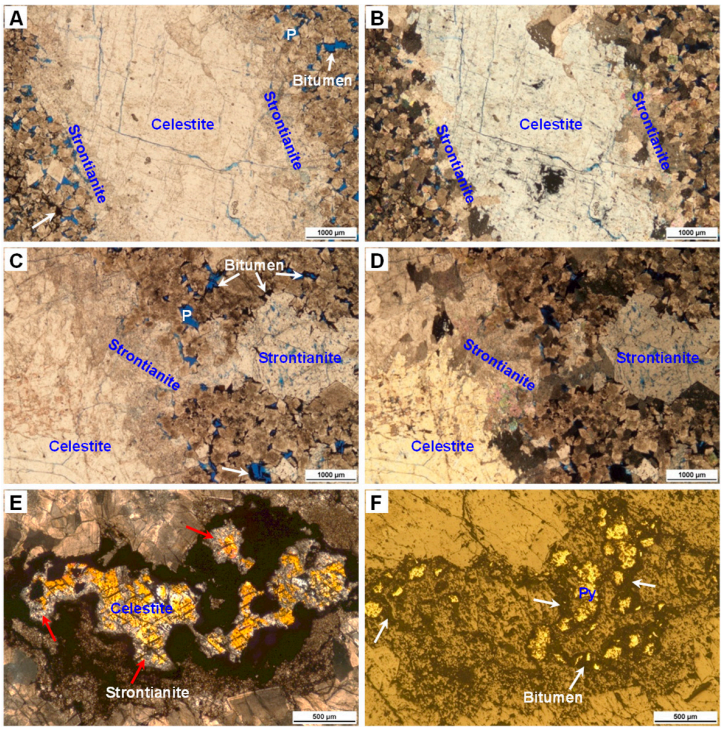

Figure 4. Thin-section photomicrographs showing the occurrence of celestites and strontianites in the YB gas field. (**A**,**B**) Celestite and strontianite minerals in the fracture of dolostone, 6640.15 m, P_3c, YB29. Note the development of solid bitumens (white arrow) in the intercrystalline pores (P) of dolomite. (**A**), under plane-polarized light (PPL); (**B**), under Cross-polarized light (CPL). (**C**,**D**) Celestite and strontianite minerals in the dissolution fracture and pore of dolostone, 6461.73 m, P_3c, YB205. Note the development of solid bitumens (white arrow) in the intercrystalline pores (P) of dolostone. (**C**), under PPL; (**D**), under CPL. (**E**,**F**) Celestites, strontianites (red arrow), solid bitumens (white arrow), and pyrites (Py) in the dolostone dissolution pore, 6583.10 m, P_3c, YB2. (**E**), under CPL; (**F**), under reflected light.

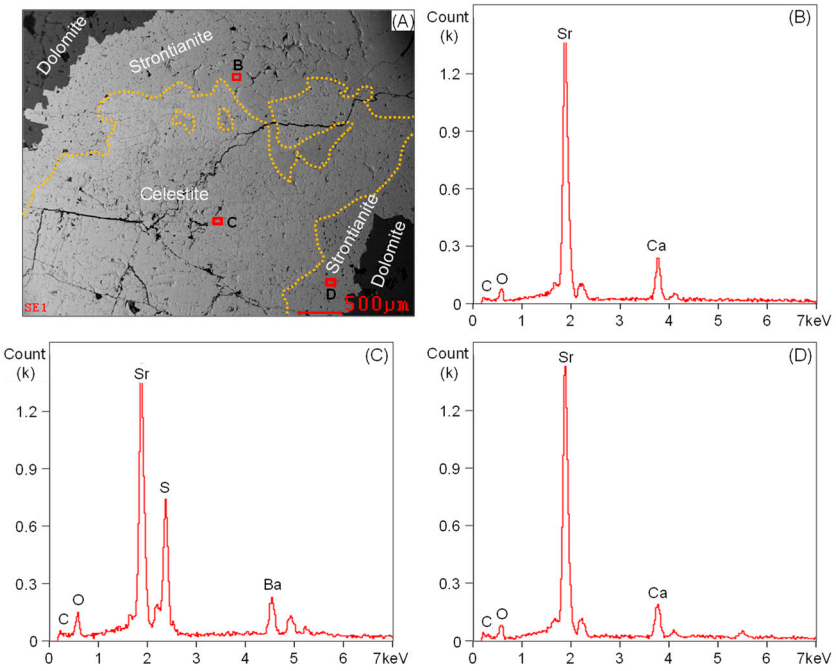

Figure 5. Back scattered electron images (**A**) and qualitative analysis of minerals of three points (**B**–**D**) in (**A**) using energy-dispersive spectrometry, 6640.15 m, P_3c, YB29.

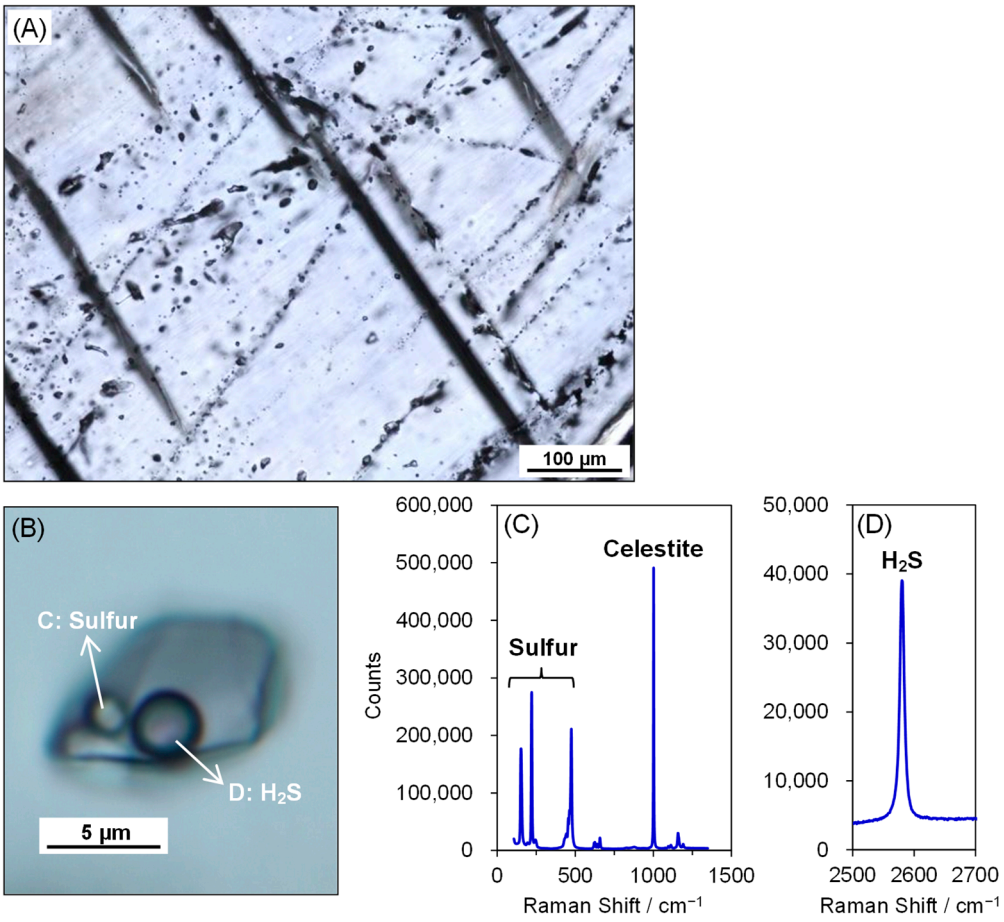

Figure 6. (**A**) Thin-section photomicrograph showing the fluid inclusions in celestite minerals of secondary origin, 6583.10 m, P_3c, YB2. (**B**–**D**) Microscopic laser Raman spectra analysis of fluid inclusions in celestite minerals, 6640.15 m, P_3c, YB29.

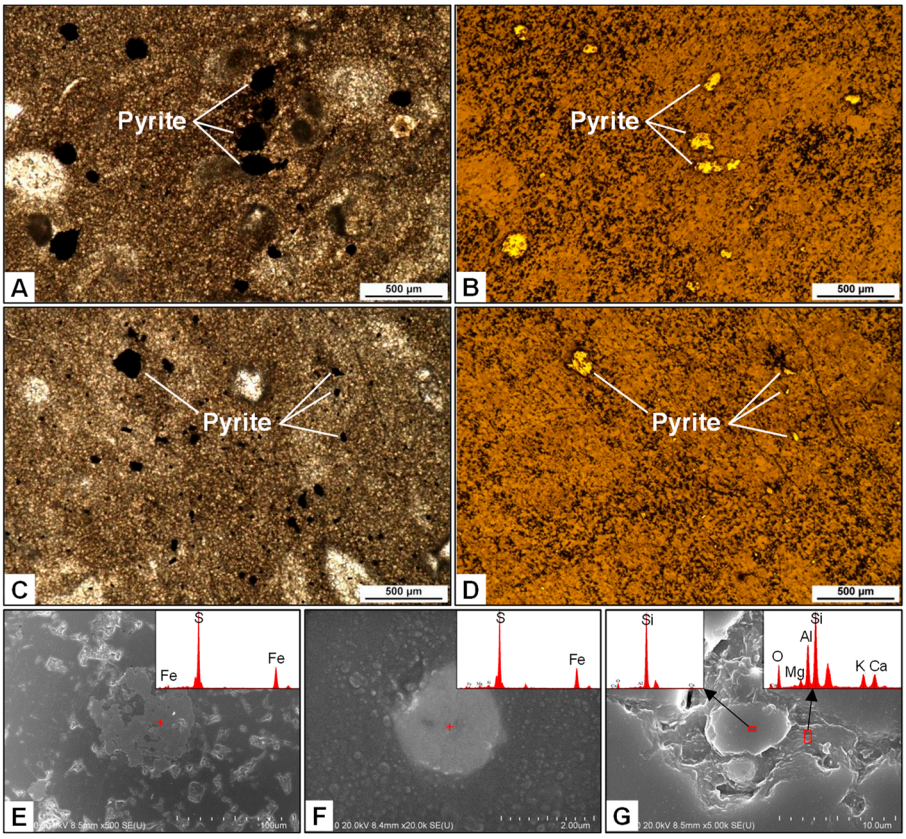

Figure 7. Thin-section and SEM photomicrographs showing pyrites and terrigenous materials near the Permian and Triassic boundary (PTB) in the well YB2. (**A**,**B**) Pyrites in dolomicrite, 6549.05 m, P_3c. (**A**), under PPL; (**B**), under reflected light. (**C**,**D**) Pyrites in dolomicrite, 6549.83 m, P_3c. (**C**), under PPL; (**D**), under reflect light. (**E**) Altered spheroidal pyrite, 6549.05 m, P_3c. (**F**) Spheroidal pyrite, 6549.83 m, P_3c. (**G**) Terrigenous clast and clay in dolomicrite, 6549.83 m, P_3c.

4.2. Sulfur and Strontium Isotopic Compositions

Three celestite samples show very heavy sulfur isotopic compositions ranging from 35.53‰ to 39.78‰, with an average of 38.05‰ (Table 1). The sulfur isotopic compositions of CAS from five dolostone samples ranged from 18.96‰ to 27.53‰, with an average of 23.61‰ (Table 2). Three limestone samples have similar CAS sulfur isotopic compositions as the dolostone samples, ranging from 19.10‰ to 26.51‰, with an average of 22.86‰. The pyrites in six dolomicrite samples from the top of the P_3c in the well YB2 showed light sulfur isotopic compositions, ranging from 1.09‰ to 10.79‰ (Table 2), with an average of 4.37‰.

Table 1. $\delta^{34}S$ and $^{87}Sr/^{86}Sr$ values for the celestite and strontianite minerals and the host rock dolostones in the P_3c in the YB gas field.

Well	Depth (m)	Sample	Occurrence	$\delta^{34}S$ (VCDT, ‰)	$^{87}Sr/^{86}Sr$
YB2	6583.10	Celestite	Vug-filling	35.53	0.707168
YB205	6461.73	Celestite	Vein-filling	38.83	0.707411
YB29	6640.15	Celestite	Vein-filling	39.78	0.707415
YB29	6640.15	Strontianite	Vein-filling	/	0.707471
YB29	6640.15	Dolostone	Matrix	/	0.707399
YB205	6461.73	Dolostone	Matrix	/	0.707396
YB2	6583.10	Dolostone	Matrix	/	0.707232

/: no data.

Table 2. $\delta^{34}S$ values for carbonate-associated sulfates (CAS) and pyrites extracted from P_3c carbonates in the YB gas field.

Well	Depth (m)	Sample	$\delta^{34}S$ (V-CDT, ‰)
YB123	6872.7	CAS in limestone	22.97
YB123	6951.9	CAS in limestone	19.10
YB224	6621.8	CAS in limestone	26.51
YB224	6640.9	CAS in dolostone	27.53
YB2	6556.6	CAS in dolostone	18.96
YB2	6559.2	CAS in dolostone	25.72
YB2	6580.6	CAS in dolostone	23.29
YB2	6584.9	CAS in dolostone	22.56
YB2	6549.1	Pyrite in dolomicrite	1.09
YB2	6549.4	Pyrite in dolomicrite	4.53
YB2	6549.7	Pyrite in dolomicrite	4.93
YB2	6549.9	Pyrite in dolomicrite	1.93
YB2	6550.0	Pyrite in dolomicrite	10.79
YB2	6550.4	Pyrite in dolomicrite	2.92

The $^{87}Sr/^{86}Sr$ ratios of the three celestite samples ranged from 0.707168 to 0.707471 (Table 1), with a wide range of variation and an average of 0.707331. The strontianite, an alteration product of celestite, has a relatively high $^{87}Sr/^{86}Sr$ ratio of 0.707471, indicating the incorporation of radioactive strontium during the alteration process. The $^{87}Sr/^{86}Sr$ ratios of the host rock dolostones range from 0.707232 to 0.707399, with an average of 0.707342. The $^{87}Sr/^{86}Sr$ ratios of the celestite samples are close to those of the host rock dolostones.

5. Discussion

5.1. Origin of Celestite

Celestite, a common but relatively minor diagenetic component of many marine carbonate platforms and reef sediments, has been extensively studied for its indicative role in depositional environments and diagenetic fluid properties. The major formation mechanisms that have been reported include: (1) Celestites precipitated in open pores by reactions between SO_4^{2-} provided by anhydrite dissolution and Sr^{2+} released during the conversion of aragonite to calcite and dolomite [42], or with Sr^{2+} provided by the dissolution of anhydrites and carbonate rocks [43]; (2) Celestites formed by replacing carbonates and evaporites [44,45]; (3) Celestites formation as a byproduct of dolomitization [44,46,47]; (4) Hydrothermal origin [48,49].

Anhydrite deposits are not developed in the P_3c and adjacent formations (P_3w and T_1f^{1-3}) in the YB gas field (Figures 1B and 2). It is therefore unlikely that the celestites in the dolostone reservoirs of the P_3c in the YB gas field were formed through the dissolution and reprecipitation of anhydrite or by the replacement of anhydrite. The YB gas field is located in the gentle tectonic zone of the northern Sichuan Basin, with weak tectonic deformation and no fault development [33,34], thus excluding hydrothermal origin. The dolomitization process can form small amounts of sulfates [50,51]. Li et al. [47] suggested that the dolomitization process and aragonite-calcite conversion in the P_3c of the YB gas field enriched in Sr^{2+} promoted the precipitation of a small number of celestites. In the following sections, the sources of Sr^{2+} and SO_4^{2-} ions of celestites in the P_3c of the YB gas field will be constrained based on the strontium and sulfur isotopic compositions.

5.1.1. Source of Sr^{2+} Ions

The $^{87}Sr/^{86}Sr$ values of celestites in the P_3c in the YB gas field are close to those of the host dolostones (Table 1; Figure 8A), indicating that the Sr^{2+} in the celestites are likely related to dolostones; in other words, the dolomitization provided Sr^{2+} for the precipitation of the celestites. There are two existing possibilities: (1) The dolomitization fluids provided the Sr^{2+} sources directly, or (2) Aragonite and calcite released large amounts of Sr^{2+} during dolomitization [47,52], which in turn provided Sr^{2+} for the precipitation of the celestites.

Regarding the former, the dolomitization fluids can be either contemporaneous or late exotic fluids. Previous studies have suggested that the Early Tiassic evaporative brines provided dolomitization fluids for the P_3c carbonates [53,54]. In contrast, Tian et al. [27] argued that the evaporative brines hardly penetrated the thick and tight limestones at the bottom of the T_1f into the P_3c, and the dolomitization fluids of the P_3c mainly derived from the contemporaneous seawater. The dolomitized T_1f oolitic shoals, which are spatially closer to the evaporate layer in the YB gas field (Figure 2), were small-scale, with thicknesses below 10 m. Most of the areas have not experienced dolomitization (Figure 9A). In contrast, large-scale dolomitization occurred in the reefs and the bioclastic shoals of the P_3c, which are far from the brine sources (Figure 9B), suggesting that the dolomitization fluids of the P_3c probably did not come from the Early Triassic evaporative brines. The CAS $\delta^{34}S$ values of dolostones (18.96~27.53‰) in the P_3c from the YB gas field are close to those of the contemporaneous limestones (19.10~26.51‰) (Figure 10) and the contemporaneous seawater (16.57~26.52‰) [55], indicating that the dolomitization fluids originated from the contemporaneous seawater.

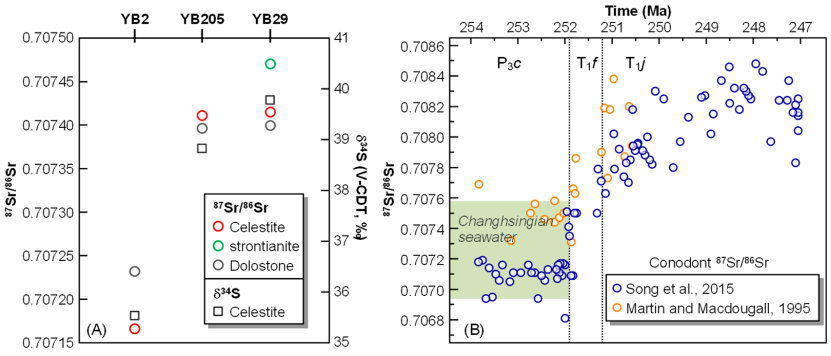

Figure 8. Comparison of $^{87}Sr/^{86}Sr$ values for celestites, strontianites, and host dolostones from P_3c in the YB gas field (**A**) and contemporaneous seawater (**B**). The $\delta^{34}S$ values of celestites are also shown in **A**. The $^{87}Sr/^{86}Sr$ values of Late Permian and Early Triassic seawater are referred to in Martin and Macdougall [56] and Song et al. [57].

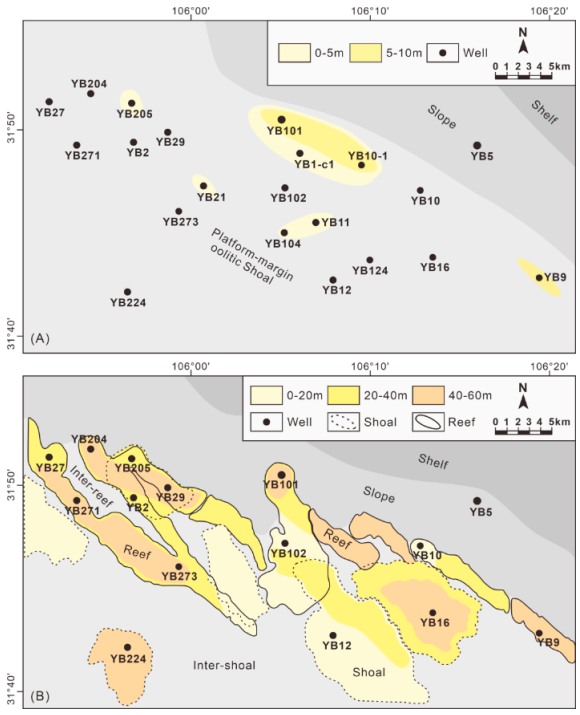

Figure 9. Distribution area and thickness of dolostones from T_1f (**A**) and P_3c (**B**) in the YB gas field. Note that the celestite samples are distributed in the northwest of the YB gas field.

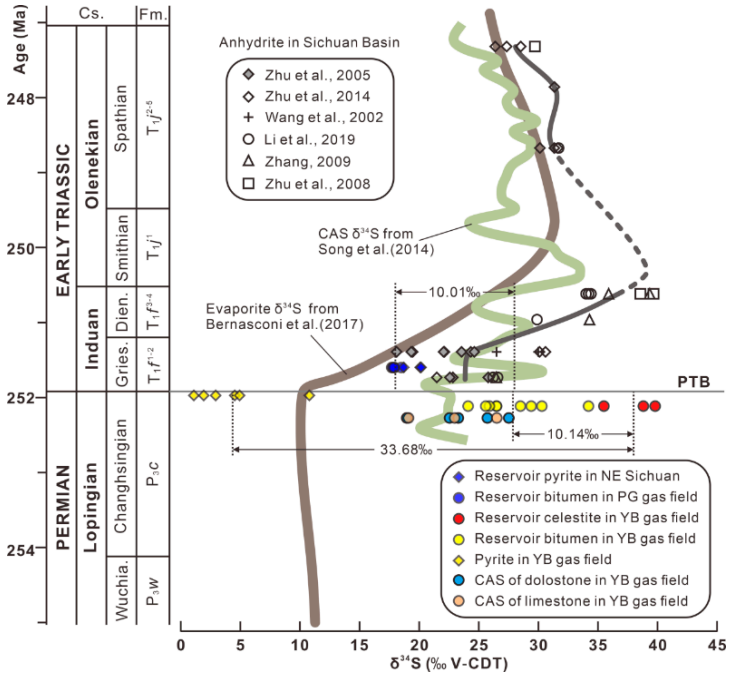

Figure 10. Comparison of $\delta^{34}S$ values for reservoir celestites, pyrites [8,58], and bitumens [26] in the P_3c and T_1f, Pyrites in PTB, CAS in the P_3c carbonates in the YB gas field, the Lower Triassic anhydrites in the Sichuan Basin [8,26,58–61], and the Late Permian and Early Triassic seawater [55,62]. The approximate correspondence between stratigraphy and geologic age is referred to un Xu et al. [63]. Cs., Chronostratigraphy; Fm., Formation; Wuchia., Wuchiapingian; Gries., Griesbachian; Dien., Dienerian.

The $^{87}Sr/^{86}Sr$ values of the P_3c celestites, strontianites, and host dolostones (0.707168~0.707471) in the YB gas field are all in the range of the $^{87}Sr/^{86}Sr$ values of the contemporaneous seawater (0.70694~0.70758) [56,57] and are significantly different from the $^{87}Sr/^{86}Sr$ values of the Early Triassic seawater (Figure 8), indicating that the Sr^{2+} in celestites are mainly derived from the contemporaneous seawater. The positive correlation between the strontium and sulfur isotopic compositions of these celestites indicates similar sources of the Sr^{2+} and SO_4^{2-}. Whether the Sr^{2+} in celestites were directly derived from contemporaneous seawater or released from aragonite and calcite during the contemporaneous seawater dolomitization needs to be determined from the sulfur isotope data.

5.1.2. Source of SO_4^{2-} Ions

The $\delta^{34}S$ values of the celestites in the P_3c dolostones in the YB gas field are significantly heavier than those of the contemporaneous seawater and the CAS $\delta^{34}S$ values of carbonate rocks at the same formation (Figure 10). Simply compared with the $\delta^{34}S$ values of T_1f^4 anhydrites, it appears that the SO_4^{2-} in the celestites originated from the evaporated brines at the late Induan or the early Olenekian. However, as mentioned earlier, this is difficult to interpret from a geologic perspective. Here, we propose an alternative possible explanation considering the special paleoenvironmental context of the end-Permian mass extinction event.

A large number of pyrite grains were found in the dolomicrites at the top of the P_3c in the well YB2 (Figure 7). The $\delta^{34}S$ values of these pyrites range from 1.09‰ to 10.79‰ (average 4.37‰), which were significantly lower than those of the contemporaneous seawater and the CAS of the P_3c carbonate rocks and were also significantly different from the reported high $\delta^{34}S$ values of the TSR-induced pyrites in the T_1f in the PG gas field (Figure 10). We propose that these pyrites distributed in the dolomicrites at the top of the P_3c in the YB gas field are of BSR origin. Previous studies have shown that BSR preferentially metabolizes light sulfur (^{32}S), causing the enrichment of heavy sulfur (^{34}S) in

the remaining sulfate [64,65]. This explains the high $\delta^{34}S$ values of the celestites in the P_3c dolostone reservoirs in the YB gas field. The −33.68‰ fractionations in the average $\delta^{34}S$ value between the pyrites and celestites in the P_3c dolostones (Figure 10) are within the range of the fractionation values during BSR (−15‰~−65‰) [21], indicating the BSR origin of these celestites.

The occurrence of the celestites filling in dissolution veins and vugs in P_3c dolostone reservoirs suggests that the celestites formed during or after dolomitization. Assuming that the SO_4^{2-}originated from the dolomitization process, the celestites should have similar $\delta^{34}S$ values as those of the CAS of the P_3c dolostones. In fact, the $\delta^{34}S$ values of the celestites are significantly higher than those of the CAS of the P_3c dolostones (Figure 10), suggesting that the SO_4^{2-} did not derive from the dolomitization process (Figure 11A). We infer that the SO_4^{2-} originated from the evaporated lagoonal seawater in the back-reef and the intershoal during the global sea-level fall at the end-Permian, which refluxed into the dissolution pores of dolostones under the combination of BSR and evaporative modifications and precipitated ^{34}S-rich celestites after mixing with Sr-rich pore water from early dolomitization (Figure 11B). The positive correlation between the $^{87}Sr/^{86}Sr$ and $\delta^{34}S$ values of the celestites suggests that these evaporative brines provided part of Sr^{2+} for the precipitation of the celestites.

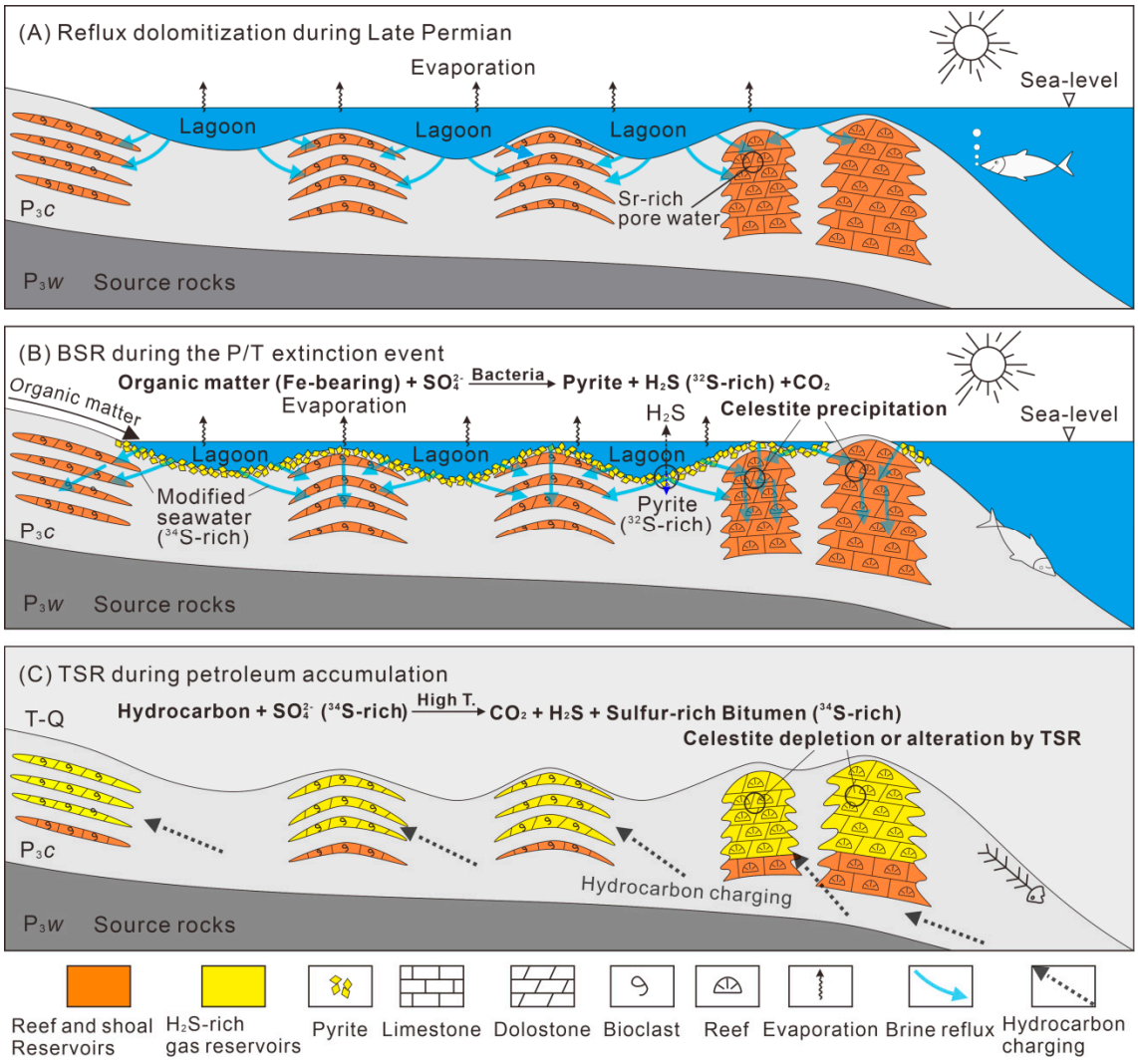

Figure 11. A schematic model for the formation of celestites, as well as the sources and evolution of sulfates. (**A**) Reflux dolomitization during Late Permian. (**B**) BSR during the P/T extinction event. (**C**) TSR during petroleum accumulation. See text fordetails. T., Temperature.

5.2. Insights into the Sulfate Required for TSR

The diagenetic effect should be considered before using the sulfur isotopic composition of celestite to decipher the source of sulfate required for TSR in the P_3c in the YB gas field. However, there is no evidence for significant diagenetic alteration of the celestite since its formation to TSR alteration, including hydrothermal alteration that can significantly affect the sulfur isotopic composition [24,66]. Thus, the sulfur isotopic composition of celestite can be used to decipher the source of sulfate required for TSR in the P_3c in the YB gas field.

The early precipitated celestites and associated fluids in the P_3c dolostone reservoirs of the YB gas field provide a sufficient source of sulfate for the intensive TSR that occurred in the late stage. The reservoir bitumens in the P_3c and T_1f of the northeast Sichuan Basin have been subjected to TSR alteration, in which the sulfur components are mainly of TSR origin [4,26], showing a heavy sulfur isotopic composition close to that of the reservoir sulfates (Figure 10). For example, in the T_1f of the PG gas field, the fractionation value of the average sulfur isotopic composition between reservoir bitumen and sulfate is 10.01‰, which is consistent with the TSR during high temperatures [21]. The fractionation value of the average sulfur isotopic composition between reservoir bitumen and celestite in the P_3c of the YB gas field is 10.14‰, which is also consistent with the TSR during high temperatures, suggesting that the celestites and related fluids provided a sulfate source for the late TSR (Figure 11B,C). Further indications of the involvement of celestite in TSR are the replacement of celestite rims by strontianite (Figures 3A, 4A–E and 5), the paragenesis of celestites with bitumens and pyrite (Figure 4E,F), and the detection of hydrogen sulfide and monatomic sulfur in the inclusions of celestite (Figure 6). It is precisely because of the alteration of celestite by TSR that the celestites are not common in the P_3c in the YB gas field. The residual celestites are only distributed in the present-day gas reservoirs in the high tectonic part of the northwest part of the YB gas field [36], where the lack of pore water prevented the occurrence of TSR [3,15], thus protecting the small number of celestites from alteration.

The formation and evolution of the celestites in the P_3c dolostone reservoirs of the YB gas field can be organized into the following three stages: (1) During the deposition of P_3c, the multistage eustastic regressions promoted the evaporation of back-reef lagoon seawater, which in turn led to reflux dolomitization in reefs and bioclastic shoals, allowing for pore water enrichment of Sr^{2+} (Figure 11A); (2) By the end of the Permian, further evaporative reflux of back-reef lagoon seawater occurred as a result of the large-scale global sea-level fall, while, at the same time, the flourishing BSR that occurred in the context of the P/T extinction event led to the enrichment of ^{34}S in evaporated seawater, which precipitated ^{34}S-rich celestites by mixing with previously Sr^{2+}-rich pore fluids (Figure 11B); (3) These ^{34}S-rich celestites and the related fluids provided a sufficient source of sulfate for the occurrence of TSR during late hydrocarbon accumulation, resulting in the heavier sulfur isotopic compositions of the present-day P_3c reservoir bitumen in the YB gas field (Figure 11C).

6. Conclusions

The celestites in the dolostone reservoirs of the Upper Permian Changxing Formation in the Yuanba gas field were not a byproduct formed during dolomitization but by direct precipitation of concentrated lagoonal brine due to the evaporation brine refluxing into the open pores of the dolostones during the end Permian regression. The heavy sulfur isotopic compositions of the celestites are the result of the bacterial sulfate reduction that occurred in the lagoonal sedimentary environment under the context of the P/T extinction event. These ^{34}S-rich celestites with associated pore fluids provide a new explanation for the source of sulfate required for the late TSR. However, it still cannot be ruled out that some evaporated brines entered the P_3c dolostone reservoirs through fractures to provide a sulfate source for the late TSR during the deposition of the T_1f^4 under shallow burial environment conditions.

Author Contributions: Conceptualization, X.Y.; methodology, X.Y. and H.Z.; software, X.Y.; validation, H.Z. and F.H.; formal analysis, X.Y.; investigation, X.Y.; resources, H.Z.; data curation, X.Y.; writing—original draft preparation, X.Y.; writing—review and editing, D.Z.; visualization, X.Y.; supervision, H.Z.; project administration, H.Z.; funding acquisition, F.H. All authors have read and agreed to the published version of the manuscript.

Funding: This research was funded by the National Natural Science Foundation of China (Grant Number 41821002).

Acknowledgments: We are grateful to the Sinopec Exploration Company, who provided support for the sample collection; the State Key Laboratory of Geological Processes and Mineral Resources (GPMR), who provided the laboratories for the analyses of strontium isotope compositions; the State Key Laboratory of Biogeology and Environmental Geology, who provided the laboratories for the analyses of sulfur isotopic compositions; the State Key Laboratory of Petroleum Resources and Prospecting in the China University of Petroleum, who provided the laboratories for SEM analysis; the Beijing Key Laboratory of Mineral Environmental Function in Peking University, who provided the laboratories for the Raman analysis of fluid inclusion. This paper benefited greatly from the critical reviews provided by three anonymous reviewers.

Conflicts of Interest: The authors declare no conflict of interest.

References

1. Orr, W.L. Changes in Sulfur Content and Isotopic Ratios of Sulfur during Petroleum Maturation—Study of Big Horn Basin Paleozoic Oils. *AAPG Bull.* **1974**, *58*, 2295–2318. [CrossRef]
2. Worden, R.H.; Smalley, P.C.; Oxtoby, N.H. Gas Souring by Thermochemical Sulfate Reduction at 140 °C. *AAPG Bull.* **1995**, *79*, 854–863. [CrossRef]
3. Machel, H.G. Bacterial and Thermochemical Sulfate Reduction in Diagenetic Settings—Old and New Insights. *Sediment. Geol.* **2001**, *140*, 143–175. [CrossRef]
4. Hao, F.; Guo, T.; Zhu, Y.; Cai, X.; Zou, H.; Li, P. Evidence for Multiple Stages of Oil Cracking and Thermochemical Sulfate Reduction in the Puguang Gas Field, Sichuan Basin, China. *AAPG Bull.* **2008**, *92*, 611–637. [CrossRef]
5. Hao, F.; Zhang, X.; Wang, C.; Li, P.; Guo, T.; Zou, H.; Zhu, Y.; Liu, J.; Cai, Z. The Fate of CO_2 Derived from Thermochemical Sulfate Reduction (TSR) and Effect of TSR on Carbonate Porosity and Permeability, Sichuan Basin, China. *Earth-Sci. Rev.* **2015**, *141*, 154–177. [CrossRef]
6. Jiang, L.; Worden, R.H.; Yang, C. Thermochemical Sulphate Reduction Can Improve Carbonate Petroleum Reservoir Quality. *Geochim. Cosmochim. Acta* **2018**, *223*, 127–140. [CrossRef]
7. Cai, C. Application of Organic Sulfur Isotopic Composition to Petroleum Origin and Evolution: A Review. *Nat. Gas Geosci.* **2018**, *29*, 159–167.
8. Zhu, G.; Zhang, S.; Liang, Y.; Dai, J.; Li, J. Isotopic Evidence of TSR Origin for Natural Gas Bearing High H_2S Contents within the Feixianguan Formation of the Northeastern Sichuan Basin, Southwestern China. *Sci. China Ser. D Earth Sci.* **2005**, *48*, 1960–1971. [CrossRef]
9. Mankiewicz, P.J.; Pottorf, R.J.; Kozar, M.G.; Vrolijk, P. Gas Geochemistry of the Mobile Bay Jurassic Norphlet Formation: Thermal Controls and Implications for Reservoir Connectivity. *AAPG Bull.* **2009**, *93*, 1319–1346. [CrossRef]
10. Jenden, P.D.; Titley, P.A.; Worden, R.H. Enrichment of Nitrogen and ^{13}C of Methane in Natural Gases from the Khuff Formation, Saudi Arabia, Caused by Thermochemical Sulfate Reduction. *Org. Geochem.* **2015**, *82*, 54–68. [CrossRef]
11. Heydari, E.; Moore, C.H. Burial Diagenesis and Thermochemical Sulfate Reduction, Smackover Formation, Southeastern Mississippi Salt Basin. *Geology* **1989**, *17*, 1080–1084. [CrossRef]
12. Worden, R.H.; Smalley, P.C.; Oxtoby, N.H. The Effects of Thermochemical Sulfate Reduction upon Formation Water Salinity and Oxygen Isotopes in Carbonate Gas Reservoirs. *Geochim. Cosmochim. Acta* **1996**, *60*, 3925–3931. [CrossRef]
13. Cai, C.; Xie, Z.; Worden, R.H.; Hu, G.; Wang, L.; He, H. Methane-Dominated Thermochemical Sulphate Reduction in the Triassic Feixianguan Formation East Sichuan Basin, China: Towards Prediction of Fatal H_2S Concentrations. *Mar. Pet. Geol.* **2004**, *21*, 1265–1279. [CrossRef]
14. Guo, T. The characteristics of sedimentation and reservoirs of reef-beach gas fields in carbonate platform margins, Northeastern Sichuan Basin. *Earth Sci. Front.* **2011**, *18*, 201–211.
15. Li, P.; Hao, F.; Guo, X.; Zou, H.; Zhu, Y.; Yu, X.; Wang, G. Origin and Distribution of Hydrogen Sulfide in the Yuanba Gas Field, Sichuan Basin, Southwest China. *Mar. Pet. Geol.* **2016**, *75*, 220–239. [CrossRef]
16. Li, K.; Cai, C.; Tan, X.; Jiang, H.; Fan, J. Massive Dolomitization Driven by $MgSO_4$-Rich Seawater and Its Effects on Thermochemical Sulfate Reduction, Upper Permian Changxing Formation, Northeastern Sichuan, China. *Energy Explor. Exploit.* **2022**, 1–29. [CrossRef]
17. Wynn, J.G.; Sumrall, J.B.; Onac, B.P. Sulfur Isotopic Composition and the Source of Dissolved Sulfur Species in Thermo-Mineral Springs of the Cerna Valley, Romania. *Chem. Geol.* **2010**, *271*, 31–43. [CrossRef]

18. Cai, C.; Li, K.; Zhu, Y.; Xiang, L.; Jiang, L.; Tenger; Cai, X.; Cai, L. TSR Origin of Sulfur in Permian and Triassic Reservoir Bitumen, East Sichuan Basin, China. *Org. Geochem.* **2010**, *41*, 871–878. [CrossRef]
19. Li, K.; Cai, C.; Hou, D.; He, X.; Jiang, L.; Jia, L.; Cai, L. Origin of High H_2S Concentrations in the Upper Permian Changxing Reservoirs of the Northeast Sichuan Basin, China. *Mar. Pet. Geol.* **2014**, *57*, 233–243. [CrossRef]
20. Krouse, H.R. Sulfur Isotope Studies and Their Role in Petroleum Exploration. *J. Geochem. Explor.* **1977**, *7*, 189–211. [CrossRef]
21. Machel, H.G.; Krouse, H.R.; Sassen, R. Products and Distinguishing Criteria of Bacterial and Thermochemical Sulfate Reduction. *Appl. Geochem.* **1995**, *10*, 373–389. [CrossRef]
22. Cai, C.; Worden, R.H.; Bottrell, S.H.; Wang, L.; Yang, C. Thermochemical Sulphate Reduction and the Generation of Hydrogen Sulphide and Thiols (Mercaptans) in Triassic Carbonate Reservoirs from the Sichuan Basin, China. *Chem. Geol.* **2003**, *202*, 39–57. [CrossRef]
23. King, H.E.; Walters, C.C.; Horn, W.C.; Zimmer, M.; Heines, M.M.; Lamberti, W.A.; Kliewer, C.; Pottorf, R.J.; Macleod, G. Sulfur Isotope Analysis of Bitumen and Pyrite Associated with Thermal Sulfate Reduction in Reservoir Carbonates at the Big Piney–La Barge Production Complex. *Geochim. Cosmochim. Acta* **2014**, *134*, 210–220. [CrossRef]
24. Zhang, P.; Liu, G.; Cai, C.; Li, M.; Chen, R.; Gao, P.; Xu, C.; Wan, W.; Zhang, Y.; Jiang, M. Alteration of Solid Bitumen by Hydrothermal Heating and Thermochemical Sulfate Reduction in the Ediacaran and Cambrian Dolomite Reservoirs in the Central Sichuan Basin, SW China. *Precambrian Res.* **2019**, *321*, 277–302. [CrossRef]
25. Jiang, X.; Xu, R.; Huang, J. Characteristics of Hydrogen Sulfide Distribution in Feixianguan Formation Gas Reservoirs in East Sichuan. *Nat. Gas Ind.* **2002**, *22*, 24–27.
26. Li, P.; Zou, H.; Hao, F.; Yu, X. Sulfate Sources of Thermal Sulfate Reduction (TSR) in the Permian Changxing and Triassic Feixianguan Formations, Northeastern Sichuan Basin, China. *Geofluids* **2019**, *2019*, 1–13. [CrossRef]
27. Tian, Y.; Ma, Y.; Liu, B.; Zhang, X.; Liu, J.; Shi, K.; Wu, S. Dolomitization of the Upper Permian Changxing Formation in Yuanba Gas Field, NE Sichuan Basin. *Acta Petrol. Sin.* **2014**, *30*, 2766–2776.
28. Zhai, G. *Petroleum Geology of China*; Petroleum Industry Press: Beijing, China, 1989; Volume 10, pp. 1–516.
29. Yao, J.; Luo, Z.; Sun, W.; Wang, R. Relationship between Emei Mantle Plume and Aulacogens of Guangwang-Kaijiang-Liangping. *Xinjiang Pet. Geol.* **2011**, *32*, 97–101.
30. Wu, Y.; Fan, J. Quantitative Evaluation of the Sea-Level Drop at the End-Permian: Based on Reefs. *Acta Geol. Sin.* **2003**, *77*, 95–102.
31. Yin, H.; Xie, S.; Luo, G.; Algeo, T.J.; Zhang, K. Two Episodes of Environmental Change at the Permian–Triassic Boundary of the GSSP Section Meishan. *Earth-Sci. Rev.* **2012**, *115*, 163–172. [CrossRef]
32. Du, J. *Natural Gas Exploration of Permian-Triassic Reef and Oolite in Sichuan Basin*; Petroleum Industry Press: Beijing, China, 2010; pp. 1–160.
33. Yu, X.; Li, P.; Zou, H.; Wang, G.; Zhang, Y. Rare Earth Element Geochemistry of Dolostones and Its Indicative Significance of the Permian Changxing Formation in Yuanba Gasfield, Northern Sichuan Basin. *J. Palaeogeogr.* **2015**, *17*, 309–320.
34. Guo, X.; Hu, D.; Li, Y.; Duan, J.; Ji, C.; Duan, H. Discovery and Theoretical and Technical Innovation of Yuanba Gas Field in Sichuan Basin, SW China. *Pet. Explor. Dev.* **2018**, *45*, 14–26. [CrossRef]
35. Guo, T. Basic Characteristics of Deep Reef-Bank Reservoirs and Major Controlling Factors of Gas Pools in the Yuanba Gas Field. *Nat. Gas Ind.* **2011**, *31*, 12–16.
36. Li, P.; Hao, F.; Guo, X.; Zou, H.; Yu, X.; Wang, G. Processes Involved in the Origin and Accumulation of Hydrocarbon Gases in the Yuanba Gas Field, Sichuan Basin, Southwest China. *Mar. Pet. Geol.* **2015**, *59*, 150–165. [CrossRef]
37. Wang, G.; Hao, F.; Zhang, W.; Zou, H.; Li, P. Characterization and Origin of Micropores in Tight Gas Grainstones of the Lower Triassic Feixianguan Formation in the Jiannan Gas Field, Sichuan Basin. *Mar. Pet. Geol.* **2022**, *139*, 105609. [CrossRef]
38. Li, C.; Planavsky, N.J.; Love, G.D.; Reinhard, C.T.; Hardisty, D.; Feng, L.; Bates, S.M.; Huang, J.; Zhang, Q.; Chu, X.; et al. Marine Redox Conditions in the Middle Proterozoic Ocean and Isotopic Constraints on Authigenic Carbonate Formation: Insights from the Chuanlinggou Formation, Yanshan Basin, North China. *Geochim. Cosmochim. Acta* **2015**, *150*, 90–105. [CrossRef]
39. Jin, C.; Li, C.; Algeo, T.J.; Planavsky, N.J.; Cui, H.; Yang, X.; Zhao, Y.; Zhang, X.; Xie, S. A Highly Redox-Heterogeneous Ocean in South China during the Early Cambrian (~529–514 Ma): Implications for Biota-Environment Co-Evolution. *Earth Planet. Sci. Lett.* **2016**, *441*, 38–51. [CrossRef]
40. Gao, S.; Rudnick, R.L.; Yuan, H.; Liu, X.; Liu, Y.; Xu, W.; Ling, W.; Ayers, J.; Wang, X.; Wang, Q. Recycling Lower Continental Crust in the North China Craton. *Nature* **2004**, *432*, 888–892. [CrossRef]
41. Xu, R.; Liu, Y.; Wang, X.; Zong, K.; Hu, Z.; Chen, H.; Zhou, L. Crust Recycling Induced Compositional-Temporal-Spatial Variations of Cenozoic Basalts in the Trans-North China Orogen. *Lithos* **2017**, *274–275*, 383–396. [CrossRef]
42. Olaussen, S. Formation of Celestite in the Wenlock, Oslo Region Norway—Evidence for Evaporitic Depositional Environments. *J. Sediment. Petrol.* **1981**, *51*, 37–45. [CrossRef]
43. Taberner, C.; Marshall, J.D.; Hendry, J.P.; Pierre, C.; Thirlwall, M.F. Celestite Formation, Bacterial Sulphate Reduction and Carbonate Cementation of Eocene Reefs and Basinal Sediments (Igualada, Northeastern Spain). *Sedimentology* **2002**, *49*, 171–190. [CrossRef]
44. Martin, J.M.; Ortega-Huertas, M.; Torres-Ruiz, J. Genesis and Evolution of Strontium Deposits of the Granada Basin (Southeastern Spain): Evidence of Diagenetic Replacement of a Stromatolite Belt. *Sediment. Geol.* **1984**, *39*, 281–298. [CrossRef]
45. Scholle, P.A.; Stemmerik, L.; Harpøth, O. Origin of Major Karst-Associated Celestite Mineralization in Karstryggen, Central East Greenland. *J. Sediment. Petrol.* **1990**, *60*, 397–410. [CrossRef]

46. Skinner, H.C.W. Precipitation of Calcian Dolomites and Magnesian Calcites in the Southeast of South Australia. *Am. J. Sci.* **1963**, *261*, 449–472. [CrossRef]
47. Li, K.; Cai, C.; Jiang, L.; Cai, L.; Jia, L.; Zhang, B.; Xiang, L.; Yuan, Y. Sr Evolution in the Upper Permian and Lower Triassic Carbonates, Northeast Sichuan Basin, China: Constraints from Chemistry, Isotope and Fluid Inclusions. *Appl. Geochem.* **2012**, *27*, 2409–2424. [CrossRef]
48. Zheng, R.; Dang, L.; Wen, H.; Chen, Z.; Chen, F.; Zhang, H. Diagenesis Characteristics and System for Dolostone in Feixianguan Formation of Northeast Sichuan. *Earth Sci.* **2011**, *36*, 659–669.
49. Meng, W.; Wu, H.; Li, G.; Zhang, X.; Lv, Z. Dolomitization Mechanisms and Influence on Reservoir Development in the Upper Permian Changxing Formation in Yuanba Area, Northern Sichuan Basin. *Acta Petrol. Sin.* **2014**, *30*, 699–708.
50. Jones, G.D.; Xiao, Y. Dolomitization, Anhydrite Cementation, and Porosity Evolution in a Reflux System: Insights from Reactive Transport Models. *AAPG Bull.* **2005**, *89*, 577–601. [CrossRef]
51. Al-Helal, A.B.; Whitaker, F.F.; Xiao, Y. Reactive Transport Modeling of Brine Reflux: Dolomitization, Anhydrite Precipitation, and Porosity Evolution. *J. Sediment. Res.* **2012**, *82*, 196–215. [CrossRef]
52. Huang, S.; Qing, H.; Pei, C.; Hu, Z.; Wu, S.; Sun, Z. Strontium Concentration, Isotope Composition and Dolomitization Fluids in the Feixianguan Formation of Triassic, Eastern Sichuan of China. *Acta Petrol. Sin.* **2006**, *22*, 2123–2132.
53. Hu, Z.; Huang, S.; Li, Z.; Zhang, Y.; Xu, E.; Qi, S. Geochemical Characteristics of the Permian Changxing Formation Reef Dolomites, Northeastern Sichuan Basin, China. *Pet. Sci.* **2013**, *10*, 38–49. [CrossRef]
54. Jiang, L.; Cai, C.F.; Worden, R.H.; Li, K.K.; Xiang, L. Reflux Dolomitization of the Upper Permian Changxing Formation and the Lower Triassic Feixianguan Formation, NE Sichuan Basin, China. *Geofluids* **2013**, *13*, 232–245. [CrossRef]
55. Song, H.; Tong, J.; Algeo, T.J.; Song, H.; Qiu, H.; Zhu, Y.; Tian, L.; Bates, S.; Lyons, T.W.; Luo, G.; et al. Early Triassic Seawater Sulfate Drawdown. *Geochim. Cosmochim. Acta* **2014**, *128*, 95–113. [CrossRef]
56. Martin, E.E.; Macdougall, J.D. Sr and Nd Isotopes at the Permian/Triassic Boundary; a Record of Climate Change. *Chem. Geol.* **1995**, *125*, 73–99. [CrossRef]
57. Song, H.; Wignall, P.B.; Tong, J.; Song, H.; Chen, J.; Chu, D.; Tian, L.; Luo, M.; Zong, K.; Chen, Y.; et al. Integrated Sr Isotope Variations and Global Environmental Changes through the Late Permian to Early Late Triassic. *Earth Planet. Sci. Lett.* **2015**, *424*, 140–147. [CrossRef]
58. Wang, Y.; Dou, L.; Wen, Y.; Zhang, J.; Liu, H. Origin of H_2S in Triassic Feixianguan Formation Gas Pools, Northeastern Sichuan Basin, China. *Geochimica* **2002**, *31*, 517–524.
59. Zhu, G.; Fei, A.; Zhao, J.; Liu, C. Sulfur Isotopic Fractionation and Mechanism for Thermochemical Sulfate Reduction Genetic H_2S. *Acta Petrol. Sin.* **2014**, *30*, 3772–3786.
60. Zhu, Y.; Wang, J.; Hao, F.; Zou, H.; Cai, X. Geochemical Characteristics and Origin of Natural Gases from Xuanhan Area, Eastern Sichuan. *Chin. J. Geol.* **2008**, *43*, 518–532.
61. Zhang, X. The Reservoir Formation and Preservation of Lower Triassic Feixianguan Formation, Northeastern Sichuan Basin. Ph. D Thesis, China University of Petroleum, Beijing, China, 2009.
62. Bernasconi, S.M.; Meier, I.; Wohlwend, S.; Brack, P.; Hochuli, P.A.; Bläsi, H.; Wortmann, U.G.; Ramseyer, K. An Evaporite-Based High-Resolution Sulfur Isotope Record of Late Permian and Triassic Seawater Sulfate. *Geochim. Cosmochim. Acta* **2017**, *204*, 331–349. [CrossRef]
63. Xu, X.; Liu, B.; Zhao, Y.; Lu, Y. *Sequence Stratigraphy and Basin—Mountain Transformation in the Western Margin of Upper Yangtze Landmass during the Permian to Triassic*; Geological Publishing House: Beijing, China, 1997; pp. 1–124.
64. Kaplan, I.R.; Rittenberg, S.C. Microbiological Fractionation of Sulphur Isotopes. *J. Gen. Microbiol.* **1964**, *34*, 195–212. [CrossRef]
65. Shen, L.; Wang, L.; Liu, C.; Zhao, Y. Sr, S, and O isotope compositions of evaporites in the Lanping–Simao Basin, China. *Minerals* **2021**, *11*, 96. [CrossRef]
66. Hoefs, J. *Stable Isotope Geochemistry*, 9th ed.; Springer: Berlin/Heidelberg, Germany, 2021; p. 504.